# Numerical investigation of laser beam-welded AA2198 joints under different artificial ageing conditions

Examilioti, Theano; Germanou, Athina; Papanikos, Paraskevas; Kashaev, Nikolai; Klusemann, B.; Alexopoulos, Nikolaos D.

23 European Conference on Fracture - ECF23

# Numerical investigation of laser beam-welded AA2198 joints under different artificial ageing conditions

T.N. Examilioti[a,b,c]*, A. Germanou[c], P. Papanikos[d], N. Kashaev[b], B. Klusemann[a,b], N.D. Alexopoulos[c]

[a]Insitute of Product and Process Innovation, Leuphana University of Lüneburg, D-21339 Lüneburg, Germany
[b]Institute of Materials Mechanics, Helmholtz-Zentrum Hereon, D-21502 Geesthacht, Germany
[c]Department of Financial Engineering, University of the Aegean, Kountourioti 41, 82 132 Chios, Greece
[d]Department of Product and System Design Engineering, University of the Aegean, Konstantinoupoleos 1, 84100 Syros, Greece

## Abstract

The present study aims to investigate the effect of weld geometry and geometrical shape imperfections on the mechanical behavior of welded joints under different post-weld heat treatment conditions. Finite element analyses were performed using the local mechanical properties of laser beam welded AA2198 joints obtained from micro-flat tensile test specimens. The finite element results show that, for the as-welded condition show that the maximum strain was observed in the lower region of the fusion zone, independently the geometrical imperfections. By applying post weld heat treatment, the maximum strain concentration can now be noticed in the upper region of the fusion zone for all the ageing times due to the lower local elongation at fracture values.

*Keywords:* Al-Li alloy, laser beam-welding, local mechanical properties, finite element model;

* Corresponding author. Tel.: +49.4131.677-1892.
E-mail address: Theano.Examilioti@stud.leuphana.de

## 1. Introduction

A significant focus of the aircraft industry is on the development of lightweight structural materials with high specific mechanical properties and good weldability (Montgomery, 2007.). Third-generation Al-Cu-Li alloys are highly promising materials with improved mechanical properties and damage-resistance behavior when compared with other commercially Al alloys such as AA2024. Rioja et al. (2012) estimated that the exploitation of high strength Al-Cu-Li alloys could reduce the structural weight by 10-15 %. The mechanical properties of Al-Cu-Li alloys are often associated with the specific volume fraction of Li and specific heat-treatment conditions (e.g., T3 or T8), which enables the formation of several strengthening precipitates besides $S$-type (Al$_2$CuMg) such as $\delta'$ (Al$_3$Li), $\delta$ (AlLi), $\theta'$ (Al$_2$Cu), and the most important $T_1$ (Al$_2$CuLi) phase (Yoshimura, 2003). Several researchers focused on the precipitation and microstructure of Al-Cu-Li alloys under different ageing conditions as well as on the effect on their mechanical properties (Decreus, 2013), (Chen, 2011).

Laser beam-welding (LBW) is a joining technique, which is already well established in the aerospace industry by replacing the conventional riveted differential structures, (Dittrich, 2011). Al-Cu-Li alloys can offer new possibilities for highly complex applications in aircraft structures by using fusion welding (Enz, 2012). To study the local mechanical properties of the welded joints, several researchers e.g., Rao et al. (2010), Ambriz et al. (2011) and Zhang et al. (2016), proposed to machine micro- flat tensile (MFT) specimens to extract the necessary mechanical properties. The investigation of the local tensile mechanical properties of LBWed Al-Li alloys using MFT specimens remains very limited as precision manufacturing of the specimens is needed. Nevertheless, the information provided is critical to predict the macroscopic behaviour of welded joints with the use of finite element model (FEM) e.g., Rao et al. (2013) and Puydt et al. (2014).

The present study focuses on the effect of different geometrical shape imperfections and artificial aging conditions post to the weld on the tensile mechanical behavior of AA2198 LBWed joints. Several imperfections such as weld bed width, weld angle, incomplete filled groove, excess weld metal, and excessive penetration, will be considered and their effect on the macroscopic tensile mechanical properties of welded joints will be assessed.

## 2. Materials and FEM input parameters

The material used in the present study is the Al-Cu-Li alloy AA2198 in T3 temper condition with a nominal thickness of 5.0 mm. Aluminum-silicon (Al-Si) 4047 wire, with a diameter of 1.2 mm, was used as filler material for all laser welded joints. The LBW parameters used in the present study were as follows: laser power $P_l$ = 8 kW, welding velocity $v$ = 6.8 m/min, resulted linear heat input HI = 70 J/mm, and wire feed rate $v_w$ = 6.0 mm/min, while in all welding processes, argon was used as shielding gas. The chemical compositions of the materials are given in **Table 1**.

Table 1. Chemical composition of investigated aluminum alloys (in wt.-%).

| Alloy | Si | Fe | Cu | Mn | Mg | Li | Zn | Zr | Ag | Ti | Al |
|-------|------|------|------|------|------|------|------|------|------|------|------|
| AA2198 | 0.03 | 0.05 | 3.35 | 0.1 | 0.32 | 0.99 | 0.1 | 0.14 | 0.27 | 0.30 | Bal. |
| AA4047 | 12.0 | 0.8 | 0.3 | 0.15 | 0.1 | - | 0.2 | - | - | - | Bal. |

The different artificial ageing heat treatments were performed post to the weld at 170 °C for different ageing times, 3 h, 48 h and 98 h, which correspond to under-ageing (UA), peak-ageing (PA) and over-ageing (OA), respectively. The artificial ageing temperature of 170 °C as well as the corresponding isothermal ageing times were selected according to Examilioti et al. (2021). The mechanical properties, which are used in the model were extracted from Examilioti et al. (2021) and (2022).

## 3. Model set up

A three-dimensional parametric FEM of the weld was developed to evaluate the effect of weld geometry and geometrical imperfections under different artificial ageing conditions. The mechanical behavior of the tensile

specimen was evaluated by conducting elasto-plastic analyses using the FE software ANSYS. Due to the symmetry of the problem at hand, only a quarter of the specimen was modelled, including symmetry conditions at the corresponding surfaces. An incremental axial displacement was applied to the free end up to a maximum nominal strain of 1.5 %, which was determined from the experimental results of Examilioti et al. (2021). The converged model consisted of approximately 23.000 elements with the size of the elements in the FZ being close to 0.2 mm. As can be seen in **Fig. 1**, the tensile test specimen was divided in 3 regions: BM, HAZ, and FZ, while FZ was divided into 3 more regions namely, top, middle, and bottom. The mechanical behavior of each region was determined from the tensile testing of micro-flat specimens in these areas. The different investigated geometrical imperfections of the weld are illustrated in **Fig. 1a-e**. The parameters which were investigated are: weld bead width (1.75 – 2.75 mm), weld angle (90 – 80º), excessive weld metal (0.3 – 0.9 mm), incompletely filled groove (0.05 – 0.25 mm) and excessive penetration (0.3 – 0.9 mm).
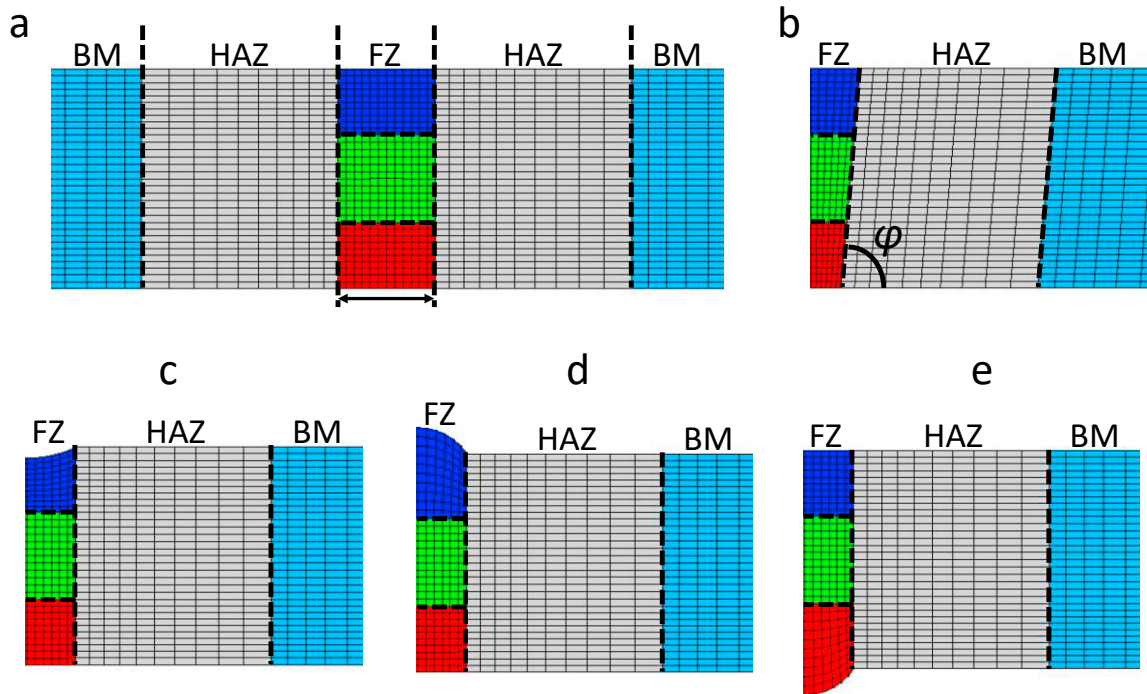


Fig. 1. Mesh detail with different colors which refers to the different volumes with different local mechanical properties for different geometrical imperfections which considered during the finite element analysis. (a) Weld bed width; (b) weld angle; (c) incomplete filled groove; (d) excess weld metal; and (e) excessive penetration.

## 4. Results and discussion

The relations between maximum equivalent strain and weld bead width of AA2198 LBWed joints under different post weld heat treatments are presented in **Fig. 2**. For the lower nominal strain of 0.5 % and with increasing artificial ageing to 98 h/170ºC, a decrease in maximum strain can be seen when compared with the as-welded condition, **Fig. 2a**. The above results can be attributed to the strain localization for the 3 and 48 h/170ºC due to lower yield stress at the top region of the weld (Examilioti, 2022). An opposite trend can be noticed for higher nominal strains of 1.0 % and 1.5 %, where the as-welded condition shows lower maximum strain when compared with the different heat-treatment conditions. As can be seen in **Fig. 2b** and **2c**, with increasing artificial ageing, PA condition presents the highest maximum strain for the lower weld bead width (1.75 mm), while with a further increase of weld bead width to 2.75 mm, a decrease in maximum strain is observed. In contrary, OA condition presents the lowest maximum strain for the lower weld bead width and respectively the highest for the higher weld bead width. Similar results

were obtained for both 80° and 90° weld angle, under different artificial ageing conditions and with increasing nominal strain from 0.5 % to 1.5 %.
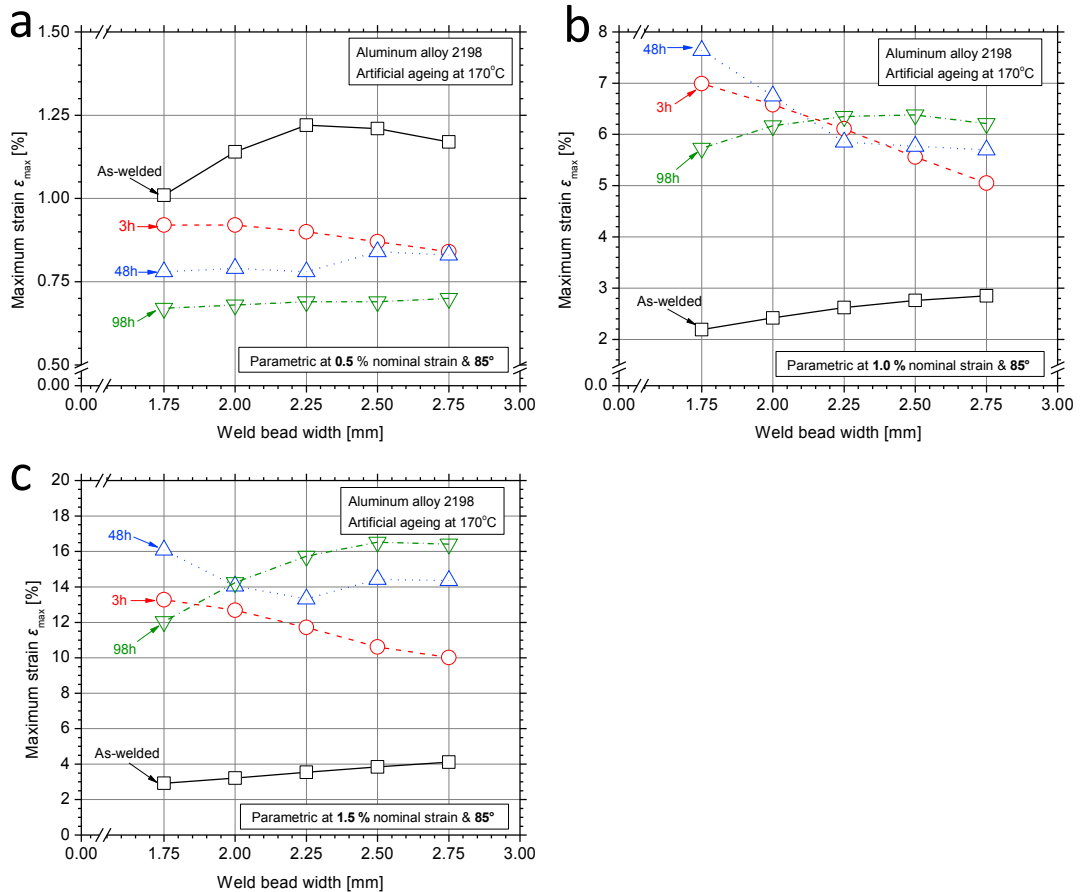


Fig. 2. Relation between maximum strain $\varepsilon_{max}$ and weld bead width for different parametric nominal strain of (a) 0.5 %, (b) 1.0 % and (c) 1.5 %, under different artificial ageing conditions for 85° weld angle.

**Fig. 3** shows the effect of the geometrical imperfections under different artificial ageing conditions for 0.5 % nominal strain. The average weld bead width (2.25 mm) and angle (85°) were kept fixed for comparison purposes. As can be seen in **Fig. 3a**, the as-welded condition did not present any significant change for the case of incompletely filled groove. With increasing artificial ageing times there is an increase of maximum strain for the incompletely filled groove by increasing the geometric shape imperfection from 0.05 to 0.25 mm. A similar trend can be noticed for the case of excessive weld metal imperfection for both as-welded and artificial ageing conditions, **Fig. 3b**. In UA and OA conditions there is a continuously increase of maximum strain from 0 up to 0.9 mm, while PA presents an increase from 0 up to 0.6 mm and then a decrease with increasing excessive weld metal imperfection to 0.9 mm, **Fig. 3b**. **Fig 3c** presents the maximum strain as compared to the excessive penetration under different artificial ageing conditions. The as-welded condition presents a slightly increase of maximum strain with increasing excessive penetration at 0.6 mm. By applying artificial ageing conditions, there is a decrease of maximum strain when compared with the as-welded condition of about 38-52 % with increasing ageing time from 3 h to 98 h/170°C. All artificial ageing curves are close to be linear independent from the geometrical shape imperfection of excessive penetration.
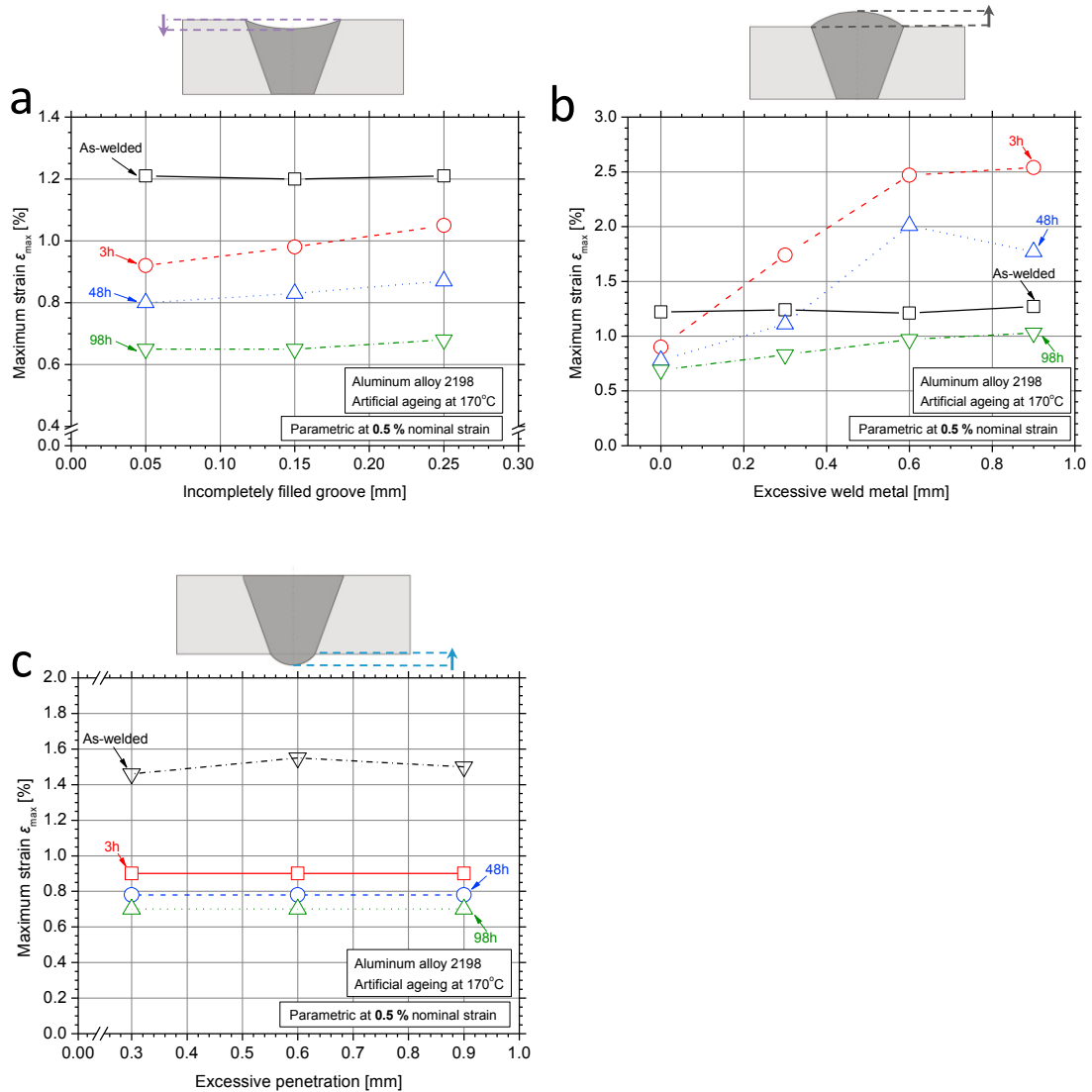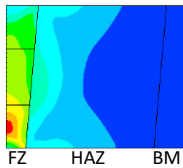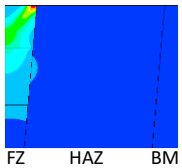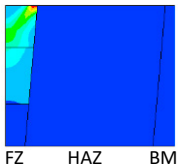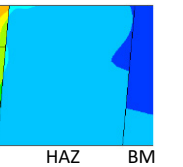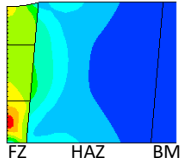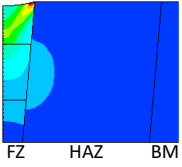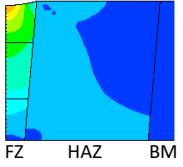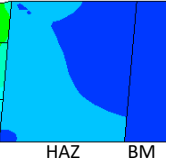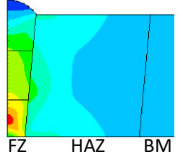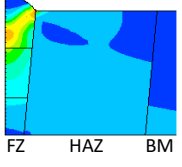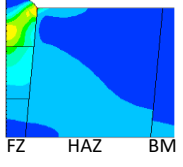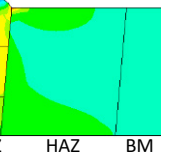
Fig. 3. Relation between maximum strain $\varepsilon_{max}$ and geometrical shape imperfections under different artificial ageing conditions for 0.5 % nominal strain. (a) Incompletely filled groove; (b) excessive weld metal and (c) excessive penetration.

The strain distribution and the position of maximum strain for the different geometrical shape imperfections and artificial ageing conditions as predicted by the model, are illustrated in **Table 2**. For comparison purposes, weld width and angle were kept fixed. In the as-welded condition, the position of the maximum strain can always be observed in the lower region of the FZ. For the welds with and without geometrical imperfections and with increasing artificial ageing to 98 h, the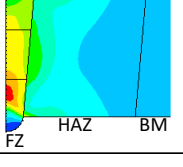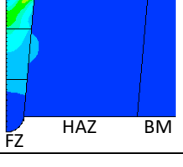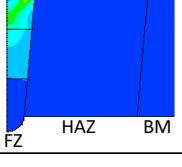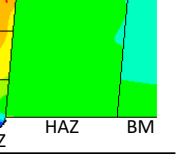 position of the maximum strain changes from the lower to the upper region of the weld seam. For the welds without geometrical imperfections and with increasing ageing time to 48 h, the maximum strain is located in the corner of the upper region of the FZ close to HAZ, while for longer ageing periods (>48 h) the maximum strain is found in the center of the upper region of the FZ. For the case of incomplete filled groove, the strain distribution in the UA condition can be noticed in the corner of the upper region of the FZ, while with a further increase of ageing the position of maximum strain located in the middle of the upper region of the FZ. A different trend can be noticed for the excessive weld metal, which shows a strain concentration in the middle of

the upper region of the FZ. The position of maximum strain is not significantly affected by the excessive penetration as it presents similar results with the welds without geometrical imperfections, independently of the PWHT conditions. The results for the weld angles of 90º show that the maximums strain was observed in the lower region of the FZ, while for the case of 80º the position of the maximum strain was observed between the upper and the middle region of the FZ. This can be attributed to the change of the weld width, which is smaller in the lower region due to the respective effect of the angle.

Table 2. Position of the maximum strain (indicated by the red color) for 0.5 % nominal strain, with weld width of 2.250 mm and weld angle of 85º, for different geometrical imperfections and artificial ageing conditions.



| Geometric imperfection parameters | | Heat-treatment condition | | | |
|---|---|---|---|---|---|
| | | As-welded | 3 h | 48 h | 98 h |
| No geometric imperfection | - | | | | |
| Incomplete filled groove [mm] | 0.15 | | | | |
| Excessive weld metal [mm] | 0.6 | | | | |
| Excessive penetration [mm] | 0.6 | | | | |

## 5. Conclusions

The effect of different weld geometries and geometrical shape imperfections of AA2198 joints on the strain distribution under different artificial ageing conditions was numerically investigated. The mechanical behaviour of each region of the fusion and heat-affected zones was modelled using locally obtained stress-strain curves from micro-flat tensile specimens. The key finding was that heat treatment changes not only the value but also the position of the maximum strain, leading to a potential different failure mode between the different welded samples. For all post weld heat treatments and with increasing ageing times up to PA, the maximum strain appears in the upper region of the FZ. A further increasing of ageing time (>48h) there is an obvious strain concentration in the upper region and especially between the FZ and HAZ.

# References

Ambriz, R.R., Chicot, D., Benseddiq, N., Mesmacque, G., de la Torre. S.D., 2011. Local mechanical properties of the 6061-T6 aluminium weld using micro-traction and instrumented indentation. European Journal of Mechanics - A/Solids, 30, 307-315.

Chen, J., Madi, Y., Morgeneyer, T. F., Besson, J., 2011. Plastic flow and ductile rupture of a 2198 Al-Cu-Li aluminum alloy. Computational Materials Science, 50, 1365-1371.

Decreus, B., Deschamps, A., De Geuser, F., Donnadieu, P., Sigli, C., Weyland. M., 2013. The influence of Cu/Li ratio on precipitation in Al–Cu–Li–x alloys. Acta Materialia, 61, 2207–2218.

Dittrich, D., Standfuss, J., Liebscher, J., Brenner, B., Beyer, E., 2011. Laser beam welding of hard to weld Al alloys for a regional aircraft fuselage design – First results. Physics Procedia, 12, 113–122.

Enz, J., Riekehr, S., Ventzke, V., Kashaev. N., 2012. Influence of the local chemical composition on the mechanical properties of laser beam welded Al-Li alloys. Physics Procedia, 39, 51-58.

Examilioti, T.N., Kashaev, N., Ventzke, V., Klusemann, B., Alexopoulos. N.D., 2021. Effect of filler wire and post weld heat treatment on the mechanical properties of laser beam-welded AA2198. Materials Characterization, 178, 111257.

Examilioti, T.N., Papanikos, P., Kashaev, N., Ventzke, V., Klusemann, B., Alexopoulos. N.D., 2022. Experimental and numerical investigation of laser beam-welded Al-Cu-Li joints using micro-mechanical characteristics, submitted for publication.

Montgomery, J., 2007. "Aircraft primary structure and materials" National Institute of Aerospace Workshop, Revolutionary Aircraft for Quite Communities, Hampton.

Puydt, Q., Flouriot, S., Ringeval, S., De Geuser, F., Estevez, R., Parry, G., Deschamps. A., 2014. Relationship Between Microstructure, Strength, and Fracture in an Al-Zn-Mg Electron Beam Weld: Part II: Mechanical Characterization and Modeling. Metallurgical and Materials Transactions A, 45, 6141–6152.

Rao, D., Heerens, J., Alves Pinheiro, G., dos Santos, J.F., Huber. N., 2010. On characterisation of local stress-strain properties in friction stir welded aluminium AA 5083 sheets using micro-tensile specimen testing and instrumented indentation technique. Materials Science & Engineering A, 527, 5018-5025.

Rao, D., Huber, K., Heerens, J., dos Santos, J.F., Huber. N., 2013. Asymmetric Mechanical Properties and Tensile Behaviour Prediction of Aluminium Alloy 5083 Friction Stir Welding Joints. Materials Science & Engineering A, 565, 44-50.

Rioja, R.J., Liu. J., 2012. The evolution of Al-Li base products for aerospace and space applications. Metallurgical and Materials Transactions A, 43(9), 3325-3337.

Yoshimura, R., Konno, T.J., Abe, E., Hiraga. K., 2003. Transmission electron microscopy study of the evolution of precipitates in aged Al–Li–Cu alloys: the h' and $T_1$ phases. Acta Materialia, 51, 4251–4266.

Zhang, X., Huang, T., Yang, W., Xiao, R., Liu, Z., Li. L., 2016. Microstructure and mechanical properties of laser beam-welded AA2060 Al-Li alloy. Journal of Materials Processing Technology, 237, 301-308.